Lead pollution recorded in Greenland ice indicates European emissions tracked plagues, wars, and imperial expansion during antiquity

Joseph R. McConnell[a,b,1], Andrew I. Wilson[c,d], Andreas Stohl[e], Monica M. Arienzo[a], Nathan J. Chellman[a], Sabine Eckhardt[e], Elisabeth M. Thompson[d], A. Mark Pollard[d], and Jørgen Peder Steffensen[f]

[a]Division of Hydrologic Sciences, Desert Research Institute, Reno, NV 89512; [b]Visiting Fellow, All Souls College, University of Oxford, OX1 4AL Oxford, United Kingdom; [c]Faculty of Classics, University of Oxford, OX1 3LU Oxford, United Kingdom; [d]School of Archaeology, University of Oxford, OX1 3TG Oxford, United Kingdom; [e]Department of Atmospheric and Climate Research, Norwegian Institute for Air Research, N-2027 Kjeller, Norway; and [f]Centre for Ice and Climate, University of Copenhagen, DK-1017 Copenhagen, Denmark

Edited by B. L. Turner, Arizona State University, Tempe, AZ, and approved April 11, 2018 (received for review December 15, 2017)

Lead pollution in Arctic ice reflects midlatitude emissions from ancient lead–silver mining and smelting. The few reported measurements have been extrapolated to infer the performance of ancient economies, including comparisons of economic productivity and growth during the Roman Republican and Imperial periods. These studies were based on sparse sampling and inaccurate dating, limiting understanding of trends and specific linkages. Here we show, using a precisely dated record of estimated lead emissions between 1100 BCE and 800 CE derived from subannually resolved measurements in Greenland ice and detailed atmospheric transport modeling, that annual European lead emissions closely varied with historical events, including imperial expansion, wars, and major plagues. Emissions rose coeval with Phoenician expansion, accelerated during expanded Carthaginian and Roman mining primarily in the Iberian Peninsula, and reached a maximum under the Roman Empire. Emissions fluctuated synchronously with wars and political instability particularly during the Roman Republic, and plunged coincident with two major plagues in the second and third centuries, remaining low for >500 years. Bullion in silver coinage declined in parallel, reflecting the importance of lead–silver mining in ancient economies. Our results indicate sustained economic growth during the first two centuries of the Roman Empire, terminated by the second-century Antonine plague.

ice core | lead pollution | plague | war | antiquity

Measurements of lead and copper in Greenland Ice Core Project (GRIP) samples (Fig. 1) first alerted historians to changes in world metal production during the last three millennia (1–3). These measurements, together with other proxy indicators, have been used in revisionist studies of the Roman economy (4–6), including suggestions that lead production during the Roman period was not exceeded until the late Middle Ages and that Republican Roman production was greater than that of Imperial Rome, indicating no economic growth during the imperial period. These findings, however, were based on only 18 discrete ice-core samples between 1100 BCE and 800 CE, each representing a 2-y average.

Studies using continuous ice-core measurements documented large temporal variability in lead deposition during recent centuries (7, 8), suggesting that ice-core records of ancient pollution were highly aliased by the sparsity of previously reported measurements (2, 3) that possibly resulted in incorrect understanding of ancient metal production and economic activity. In addition, substantial dating uncertainties in early ice-core studies, and even larger decades-to-centuries uncertainties in other paleo-environmental archives (9–13), precluded precise linkages to historical events.

High-Resolution Record of Greenland Lead Pollution

Nearly contiguous, subannually resolved new measurements of lead pollution in Greenland ice provide a much more complete and accurate emissions record during antiquity (Fig. 2*B* and Fig. S1). This 1235 BCE to 1257 CE record was developed using a continuous ice-core analytical system (7, 8, 14) to measure a broad range of chemical species in 423 m of archived North Greenland Ice Core Project (NGRIP2) (Fig. 1) ice core, with protocols adjusted to target lead (*Materials and Methods*). Pollution lead concentrations and fluxes were derived by subtracting estimated background lead (15) from the measured totals (*Materials and Methods*).

Accurate chronologies are required for quantitative linkages to historical events so we used the NGRIP2 measurements and an annual-layer-counting approach (Fig. 2) to develop an independent Greenland ice-core chronology (DRI_NGRIP2), with an estimated overall uncertainty of 1 to 2 y during antiquity (*Materials and Methods*). Comparisons of the DRI_NGRIP2 chronology to recently reported NEEM_2011_S1 (14) and IntCal13-based (16) (Fig. S2) chronologies showed minor differences that were well within their respective uncertainties (*Materials and Methods*). Comparisons of the 18 synchronized GRIP discrete lead measurements (2) with the new annual NGRIP2 lead-concentration record showed general agreement, despite the ∼300-km separation between drilling locations (Fig. 2).

Lead Pollution Provenance and Estimated Emissions

The utility of Greenland ice cores for investigating ancient economies assumes that European lead emissions largely from

Significance

An 1100 BCE to 800 CE record of estimated lead emissions based on continuous, subannually resolved, and precisely dated measurements of lead pollution in deep Greenland ice and atmospheric modeling shows that European emissions closely varied with historical events, including imperial expansion, wars, and major plagues. Emissions rose coeval with Phoenician expansion and accelerated during expanded Carthaginian and Roman lead–silver mining primarily in the Iberian Peninsula. Emissions fluctuated synchronously with wars and political instability, particularly during the Roman Republic, reaching a sustained maximum during the Roman Empire before plunging in the second century coincident with the Antonine plague, and remaining low for >500 years. Bullion in silver coinage declined in parallel, reflecting the importance of lead–silver mining in ancient economies.

Author contributions: J.R.M., A.I.W., A.S., and A.M.P. designed research; J.R.M., A.I.W., M.M.A., N.J.C., S.E., and E.M.T. performed research; J.R.M., A.I.W., A.S., M.M.A., N.J.C., S.E., A.M.P., and J.P.S. analyzed data; and J.R.M., A.I.W., and A.S. wrote the paper.

The authors declare no conflict of interest.

This article is a PNAS Direct Submission.

[1]To whom correspondence should be addressed. Email: Joe.McConnell@dri.edu.

This article contains supporting information online at www.pnas.org/lookup/suppl/doi:10.1073/pnas.1721818115/-/DCSupplemental.

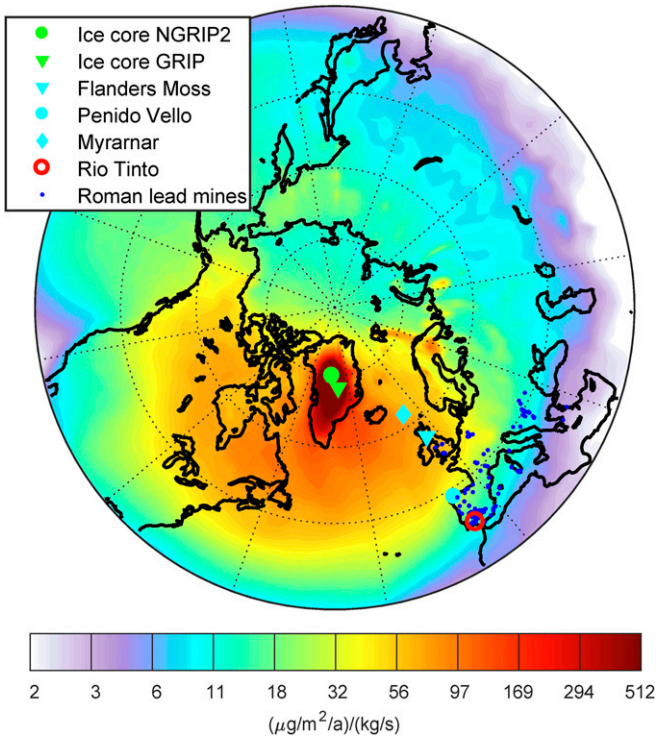

Fig. 1. Sensitivity (23) of the NGRIP2 ice-core record to Northern Hemisphere atmospheric lead emissions from FLEXPART (20) transport model simulations. Also shown are locations of the NGRIP2 and GRIP ice cores (green), three peat bog coring sites (cyan), where historical lead records were evaluated, and Roman-era mine sites (blue) including Rio Tinto (red).

mining and smelting of lead–silver sulfide ores (e.g., galena) dominated other sources during antiquity (17, 18). At the Roman mines of Rio Tinto in Spain, for example, crushed lead–silver ores were roasted and smelted at ∼1,200 °C for some 10 h in small, hemispherical clay furnaces. Furthermore, lead was added to concentrate the silver, and the argentiferous lead was run off and subsequently cupelled to separate the lead and silver (19). Most of the emissions resulted from high-temperature smelting. Lead isotopic ratios in the few reported discrete GRIP samples were consistent with sources in Spain, as well as northwestern and central Europe (2).

To investigate transport of pollution to Greenland, we used the atmospheric transport and deposition model FLEXPART and assumed that atmospheric transport during antiquity was similar to the 20th century when meteorological fields required for modeling were available (*Materials and Methods*) (20). In agreement with the lead isotope measurements (2), simulations (Fig. 1) indicated that lead deposition at the NGRIP2 site indeed was dominated by ancient European mining and smelting emissions (21) (*Materials and Methods*). Transport from other potential ancient emission sources (e.g., in China) was nearly an order of magnitude less efficient (Fig. 1), thus requiring unrealistically high emissions from these other sites (18) to overwhelm the European signal.

We also evaluated the spatial and temporal patterns of European-region lead deposition using previously published peat bog records (*Materials and Methods*). Comparisons showed that temporal changes in the NGRIP2 ice core paralleled those in the peat bogs within their dating uncertainties, suggesting common primary emission sources during classical antiquity (Fig. S5). Moreover, the relative magnitudes of the Roman era lead pollution observed in peat bog and Greenland ice archives, and simulated using FLEXPART (*Materials and Methods*), suggested that these common primary sources were located in southern Europe (Fig. S6).

Lead–silver ore processing is directly linked to silver production, an important driver of ancient economies (4, 22). Lead pollution serves as an economic indicator of lead and silver mining and smelting output, and may be considered a proxy of wider economic performance particularly when silver is a key component of currency. Using FLEXPART-simulated average transport and deposition (20, 23), we converted the NGRIP2 record to estimated lead emissions with a factor of two estimated uncertainty in the overall conversion factor based on differences in how specific aerosol types were transported through the atmosphere (*Materials and Methods*). The FLEXPART simulations also indicated year-to-year relative variability (1 σ) of 58%, so to reduce impacts of interannual transport and deposition variability while preserving any step-function changes in historical emissions, we evaluated the annual lead emissions after filtering with an 11-y median filter (Fig. 3).

Historical Linkages

Sustained increases in lead emissions began ∼1000 BCE, coincident with Phoenician expansion into the western Mediterranean (Fig. 3), and continued through the late second-century BCE as mining activities increased (24, 25), particularly in the western and northern Mediterranean where FLEXPART modeling suggested high emissions sensitivity in the NGRIP2 record (Fig. 1).

Sustained high emission levels in the mid-fourth to second centuries BCE corresponded to intensive mining in Carthaginian and Republican Roman Spain, and in the first and second centuries CE to mining under the Roman Empire. Fluctuations within the overall pattern corresponded to wars affecting key mining regions (Fig. S7 and Table S1), with short-term declines probably caused by the diversion of some of the mining workforce to warfare, or by flight from mining regions affected by warfare. Longer-term declines possibly were linked to disincentives to investment in war-torn regions. For example, lead emissions dropped notably at the outbreak of the first Punic War (264–241 BCE) but rose in the later years as Carthage increased its minting of silver coin to pay mercenaries (26). During the Second Punic War, lead emissions initially declined but rose after Rome seized Carthaginian mining territories in southern Spain in 206 BCE (27).

Warfare between 200 and 79 BCE in the Iberian Peninsula and southern France also corresponded to downturns in lead emissions. For example, emissions dropped sharply after 125 BCE, contemporary with warfare in south-central France against the Allobroges (124 BCE) and the Arverni (124–121 BCE), as well as invasions by the Cimbri and Teutones in 104–101 BCE. They remained low during recurrent warfare in Spain from 108 to 82 BCE (Table S1). A further drop after 80 BCE to the sustained Republican minimum coincided with the Sertorian War in Spain (80–72 BCE), and emissions remained low during the next decade coincident with periodic Lusitanian raids (72–62 BCE). A marked recovery began only after 61 BCE when Julius Caesar, then governor of Spain, campaigned against the Lusitanians to restore order (28). This recovery was sustained for about 10 y, but arrested and reversed during the Civil Wars, from Caesar's campaigns in Spain (49–46 BCE) until the eventual victory of Octavian/Augustus (31 BCE). The repeated pattern of dips in production coinciding with the outbreak of wars primarily affecting the Iberian Peninsula, and then recovery again after the end of each war, suggests that warfare caused major interruptions to lead–silver production during the middle and late Roman Republic. The Crisis of the Roman Republic characterized by repeated wars and political instability from the late second- to mid–first-century BCE coincided with a sustained period of very low lead emissions.

A peace dividend after the Civil Wars reversed the late second- to mid–first-century BCE decline, with the highest lead emissions in antiquity occurring in the first-century CE, rather than the first-century BCE, as suggested by the few GRIP samples (2, 3). Following a rapid rise in emissions starting in 17 BCE, emissions remained high until the 160s, again with short-term fluctuations. This period of high emissions coincided with the apogee of the Roman Empire under the Pax Romana, marked at its start by the consolidation of imperial rule over the provinces, and at its end by the devastating Antonine plague, probably smallpox, from 165 to 193 CE (29).

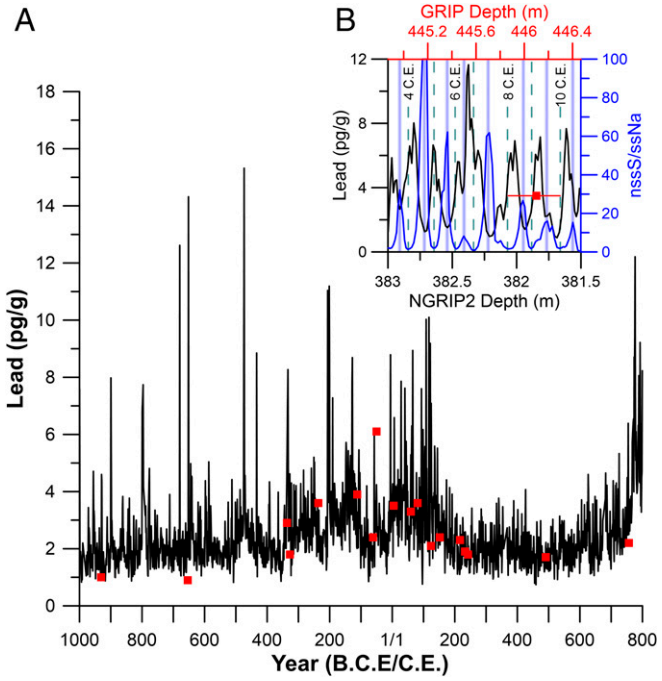

Fig. 2. Lead measurements in Greenland ice. (*A*) Nearly contiguous 1000 BCE to 800 CE annual average lead measured in the NGRIP2 ice core compared with the 18 previously reported discrete lead measurements from the GRIP core (red squares) (2) on the new DRI_NGRIP2 chronology with an estimated overall uncertainty of 1 to 2 y during antiquity (*Materials and Methods*). (*B*) Typical high-resolution lead measurements in depth with the non–sea-salt sulfur/sea-salt sodium (nssS/ssNa) ratio that was one of several parameters used for annual-layer counting. Midwinter depths assigned to years 4–10 CE are shown. The discrete lead measurements in the GRIP core (2) each represented 2 y of snowfall.

Much of the imperial period rise in emissions may be attributed to exploitation of mines in northern Spain following the conquest of Asturia and Cantabria, completed by 16 BCE, and in Germany on both sides of the Rhine from 8 BCE onwards. Although there were fewer Roman mines here than in southern Spain, FLEXPART simulations indicated NGRIP2 emissions sensitivities in these regions were greater than in Cartagena and the Sierra Morena (Fig. S6): by a factor of two to three at sites in the very north of Spain, two at sites in Germany west of the Rhine, and as high as five in the Sauerland east of the Rhine. The decline from the highest first-century CE peak occurred in 9 CE, coincident with Roman abandonment of territory to the east of the Rhine, including the Sauerland mines, after three legions were annihilated in the Teutoburg forest. After the mid–first-century CE, the sustained Roman imperial peak probably resulted from emissions from mines throughout Spain and in south-central Gaul, Britain, and Germany. Variations within the imperial period reflected the rise and decline of mining areas in some of these regions, especially those where NGRIP2 emissions sensitivities were particularly high.

The Antonine plague marked the turning point between high levels of lead–silver production during the Roman Empire period and much lower levels observed from the mid-second century until the mid-eighth century. The plague disrupted mining through high mortality in, and flight from, mining regions, and reduced demand through population loss. The period of lowest emissions at any time after 900 BCE coincided with the third-century Imperial Crisis from 235 to 284 CE, and in particular with the severe pandemic known as the Plague of Cyprian (249–270 CE) (29). The first major recovery in lead emissions after the Antonine plague occurred ∼750 CE, with resumption of early medieval mining in France, notably the Merovingian mine and mint at Melle, and in Britain around Wirksworth in Derbyshire (30).

The fluctuations in lead–silver mining and smelting indicated by the Greenland lead pollution record and estimated lead emissions were directly reflected in the fineness and metallurgy of Rome's silver coinage, the denarius (Fig. 3). A sharp drop in lead emissions coincided with debasement of the denarius silver content in 64 CE and a switch in denarii production from new metal to recycling coinage. Similarly, a short-lived peak in the early second-century CE coincided with a brief period of new metal use again (103–107 CE) (31). The final debasement of the denarius in the third-century CE to a silver content of under 4% coincided with the absolute nadir in lead emissions in our record after 900 BCE; from the late-third to the mid–fourth-century CE, the Roman monetary system shifted to essentially a bimetallic currency in gold and copper alloy, with only brief exceptions when silver coin was issued (4).

Conclusion

Our subannually resolved, precisely dated record of estimated European lead emissions provides a much more accurate and detailed history of lead–silver mining and smelting activities during antiquity, and reflects both periods of prosperity and economic disruption. Especially striking are the very low levels of lead pollution during the last decades of the Roman Republic, characterized by wars and political unrest known as the Crisis of the Roman Republic, the nearly fourfold higher levels during the Pax Romana at the apogee of the Roman Empire, indicating substantial economic growth compared with the late Republican period, and the pronounced and lasting declines during the two great pandemics of Roman antiquity in the second century (Antonine plague) and third century (Plague of Cyprian). The Antonine plague emerges as an abrupt transition, marking the end of high lead emissions in Europe and ushering in a period of much lower lead–silver production lasting more than five centuries. Unlike the recently reported response to the 14th-century Black Death pandemic (32), the nearly immediate and persistent emissions declines following major plague outbreaks suggest low societal resilience and far-reaching economic effects (29).

Materials and Methods

Continuous Measurements of the NGRIP2 Ice Core. The bedrock NGRIP2 ice core (75.1°N, 42.32°W, 2,917 m) was collected beginning in 1998 adjacent to the intermediate NGRIP core (33). For this study, longitudinal samples (∼1.0 by 0.035 by 0.035 m) from 159.56 to 582.43 m depth were cut in 2015 from the University of Copenhagen's NGRIP2 archive and analyzed using the Desert Research Institute's (DRI's) continuous melter system (7, 8, 14, 34, 35).

The DRI ice-core analytical system includes two Element2, high-resolution inductively coupled plasma mass spectrometers (HR-ICP-MS) operating in parallel, along with a host of other instruments for continuous, near real-time, simultaneous measurements of ∼30 elements, isotopes, and chemical species (34, 36, 37). All measurements were exactly coregistered in depth. Different configurations of the DRI analytical system have been used to target specific research objectives (7, 8, 36, 38, 39). For this study, one HR-ICP-MS was used in low-slit resolution and electronic scan mode to measure a narrow range of elements that included only thallium, lead, and bismuth, with 60 individual ^{205}Tl to ^{209}Bi mass scans combined to yield one sample. The second HR-ICP-MS was used in medium-slit resolution to measure 14 elements, including indicators of sea salts (sodium, magnesium, chlorine), marine biogenic emissions, and volcanic fallout (sulfur), and continental dust (calcium, cerium), as well as lead, with one ^{23}Na to ^{208}Pb mass scan comprising a single sample. The full record between 159.56 and 582.43 m included >21,000 low (average of ∼9 samples/a) and >48,000 medium (average of ∼19 samples/a) slit resolution measurements of lead, respectively. Mixing within the continuous flow system resulted in smoothing between the individual HR-ICP-MS measurements, leading to an effective depth resolution for the HR-ICP-MS measurements of ∼0.015 m, equivalent to ∼12 samples/a during the Roman era.

Lead concentration detection limits (defined as three times the SD of the blank) using these configurations for the low- and medium-slit resolution instruments were ∼0.01 and ∼0.18 pg/g, respectively, well below the average NGRIP2 lead concentrations of ∼1.4 and ∼3.0 pg/g during background (1100–1000 BCE) and Roman periods, respectively. Concentrations ranged from

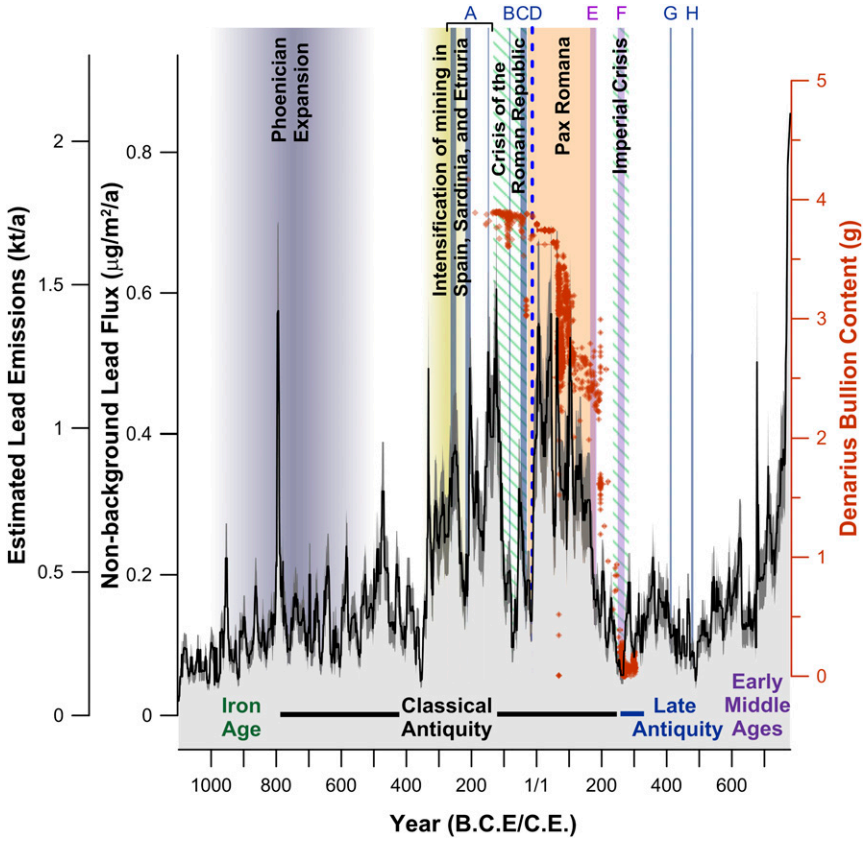

Fig. 3. Nonbackground lead deposition in Greenland ice and estimated European lead emissions, silver bullion content in coinage, and selected historical events during antiquity. Gray shading indicates 22% uncertainty (1 σ) in estimated annual emissions after 11-y median filtering based on year-to-year variability in FLEXPART-simulated atmospheric transport (*Materials and Methods*). We estimate a factor of two uncertainty in the overall magnitude of lead emissions. Estimated annual emissions derived from the measured annual lead deposition record ranged from 0.3 to 3.8 kt/a and averaged 1.1 kt/a during the first-century apogee of the Roman Empire, comparable to previous, less quantitative peak emissions estimates during this period of 4 kt/a, based only on historical and archeological evidence and a roughly estimated 5% emissions factor (3). Also shown are the changing silver bullion content of Roman denarius coins (31), periods of major wars and plagues thought to have affected mining regions of southern Spain (Table S1), and selected historical events (A: Punic Wars, B: Sertorian War, C: Civil Wars, D: Final pacification of Gaul and Spain, E: Antonine plague, F: Plague of Cyprian, G: Roman abandonment of Britain, H: Collapse of the Western Roman Empire).

0.40 pg/g to more than 20 pg/g during these periods. The much more precise, low-slit resolution measurements of lead were used throughout this study.

Pollution lead was derived from the total lead concentrations measured in the NGRIP2 core by assuming that total lead was comprised of three components: crustal lead from windblown dust, volcanic lead largely from quiescent emissions (40), and pollution lead (7). To derive crustal lead, we multiplied the annual average cerium concentrations by a published "mean sediment" value for the lead to cerium ratio of 0.23 (41). Assessment of measurement recovery during continuous measurements of NGRIP2 with the DRI analytical system indicated that recovery was ∼100% and ∼60% for lead and cerium, respectively (Fig. S8). Therefore, measured cerium concentrations were scaled by a factor of 1.7 to correct for underrecovery (36, 42, 43); no correction for lead was necessary.

Crustal lead was subtracted from measured total lead to yield noncrustal lead that included both the volcanic and pollution components. Lacking any independent indicator of fallout from quiescent volcanic emissions in our measurements, we assumed that the volcanic lead component was constant throughout the record. To estimate the maximum constant volcanic lead component consistent with our measurements, we averaged those years with the lowest noncrustal lead concentrations on the assumption that pollution lead was negligible during those specific years. We chose to average the lowest 5% of the >2,000-y record which, while somewhat arbitrary, yielded a constant volcanic lead component of 0.33 pg/g. For perspective, the average measured total lead and derived crustal lead concentrations were 2.44 and 0.93 pg/g, respectively, so the constant volcanic component represented ∼27% of the background (crustal + volcanic) lead concentration consistent with global estimates (44, 45) and only ∼13% of the total lead measured in the NGRIP2 core.

Nonbackground or pollution lead was derived by subtracting the background lead from the total measured lead. Implicit in using the average of the 5% of years with the lowest noncrustal lead concentrations to derive the constant volcanic component was that some of the annual pollution lead values were negative.

Following standard procedures (36), the depositional flux of nonbackground lead (Fig. S1) was calculated as the product of the nonbackground lead concentration and the annual water equivalent snow accumulation determined from the annual-layer thicknesses in the core corrected for flow thinning (46).

Lead enrichment (Fig. S1) is an indicator of relative abundance and was calculated following standard procedures (8, 36), as the ratio of lead to cerium measured in the ice core divided by the ratio for mean sediment. Here we used a mean sediment ratio of 19/83 (41). Enrichment of 1.0 indicated that all lead measured in the ice could be attributed to continental dust.

To minimize potential lead contamination, all sections of the NGRIP2 core containing visible fractures or other physical damage were set aside and not measured during the primary analyses, and so were not included in the lead record. Instead, those sections were analyzed later, and the measurements inserted into the sea salt, continental dust, and other chemical records used for dating. The result was reliable lead measurements for 89% of the 420.34 m between 162.09 and 582.43 m, with most missing sections corresponding only to a few months of the record, and 94% for most of the other chemical concentrations used for annual-layer counting and dating. To further complete the record used for annual-layer counting, previously reported discrete (0.05-m depth resolution) chemical measurements from the NGRIP core from 159.5 to 349.8 m, approximately corresponding to 1260–190 CE (47), were synchronized to NGRIP2 and inserted into the NGRIP2 record to fill in the few longer sections of missing measurements.

New Independent Ice-Core Chronology for NGRIP2. Significant progress recently has been made in improving Greenland ice-core chronologies and linking them to other well-dated archives, such as tree-ring sequences (14, 16). Because the continuous NGRIP2 measurements did not extend to the surface, here we used the distinct sulfur concentration maximum associated with the well-known Samalas volcanic eruption to synchronize the uppermost NGRIP2 measurements to the NEEM_2011_S1 volcanic record (14) at 1257 CE. The remaining 162.09- to 582.43-m NGRIP2 record was independently dated through annual-layer counting to provide a nearly contiguous history of lead concentration, enrichment, and deposition from 1235 BCE to 1257 CE. A multiparameter approach was used in the annual-layer counting (7, 14), with annual variations in a number of chemical and elemental concentrations (e.g., non–sea-salt calcium, insoluble particle counts) as well as the non–sea-salt sulfur to sea-salt sodium ratio (Fig. 2*B*) employed to robustly identify annual time horizons.

Comparisons of the timing of major volcanic sulfur deposition events using our independently derived DRI_NGRIP2 chronology and the previously reported Greenland ice-core chronology largely based on the intermediate NEEM_2011_S1 and bedrock NEEM cores (14), showed only minor (typically 0 to 2 y) differences that were well within the uncertainties of the published NEEM chronology (14). Note that while both records were developed largely using continuous measurements from DRI's ice-core analytical system, the NGRIP2

record was more complete in depth coverage because the quality of the original ice-core samples was higher, particularly for the bedrock NEEM core portion of the previously published record (before 87 CE), which was damaged in shipping, leading to a more accurate DRI_NGRIP2 chronology (14).

Further evaluation of the new DRI_NGRIP2 chronology came from comparisons to an independent Greenland ice-core age scale developed using cosmogenic nuclides (16), specifically the IntCal13 record of carbon isotopes (^{14}C) in well-dated, tree-ring sequences and measurements of beryllium isotopes (^{10}Be) in the GRIP ice core (Fig. S2). Differences were only 1 to 2 y and within the 1 σ confidence intervals for the IntCal13-based chronology.

Comparisons Between Continuous NGRIP2 and Discrete GRIP Lead Measurements. The 18 GRIP discrete lead measurements (2) were reported on an earlier GRIP timescale that was substantially different from current chronologies (16), so direct comparisons to the new NGRIP2 continuous measurements required synchronization of the GRIP and NGRIP2 ice-core chronologies. Using published, high-depth-resolution, dielectric profiling measurements in the GRIP core (48), and our continuous NGRIP2 sulfur measurements, we identified 137 unambiguous volcanic tie points in the two records between 1235 BCE and 1270 CE and used them for synchronization (49). Comparisons to the original GRIP copper, lead, and lead isotope chronology (1–3) showed differences of up to 31 y, with the largest differences in the first-century BCE (Fig. S3). Comparisons of the new annual record of lead concentration to the 18 previously published discrete lead measurements (2) showed general agreement (Fig. 2), despite the ∼300-km separation between the drilling locations (Fig. 1).

Provenance of Greenland Lead Pollution During Antiquity. Lead isotopic ratios in the few previously reported discrete samples of GRIP ice were consistent with Roman-era mining and smelting operations in Spain, as well as northwestern and central Europe, as the primary sources of pollution lead during classical antiquity (2). To better understand and quantify potential sources of pollution lead deposited in north central Greenland, we evaluated published lead depositional fluxes in three western European peat bog records: Myrarnar, Faroe Islands (11); Flanders Moss, Scotland (10); and Penido Vello, Spain (9, 50). Although discontinuously sampled and with uncertainties in the ^{14}C-based ages ranging from decades to centuries, all three peat bog records showed similar temporal variability to the NGRIP2 lead record (Fig. S3), suggesting common primary emission sources during classical antiquity. Note that Roman-era mining and smelting previously have been inferred to be the dominant sources of lead pollution in all three bogs (9–11, 50), sometimes supported by lead isotopic evidence (9–11).

Deposition rates decline approximately exponentially with distance from the source. If the common emission sources during antiquity were European, then lead pollution fluxes would be substantially (one-to-three orders-of-magnitude) higher in proximal records (e.g., western European peat bogs) compared with distal records (e.g., the NGRIP2 ice core in Greenland) that would not be the case for distant emissions sources, such as in Asia. Fluxes of noncrustal lead in the European peat bog records during the first-century CE were on the order of 100–1,000 μg/m^2/a, or 300–3,000 times the ∼0.33 μg/m^2/a measured in the NGRIP2 core. Fluxes to the peat bogs during the Roman era generally declined exponentially with distance from southern Spain, consistent with primary sources in the Rio Tinto region. While ice cores record wet and dry deposition directly and so closely reflect atmospheric concentrations, deposition and postdeposition processes in peat bogs are more complex (51), so fluxes recorded in peat bogs often are not as directly linked to atmospheric concentrations. Moreover, local sources of lead emissions—such as those reported for Flanders Moss, Scotland (10) and Penido Vello, Spain (9)—probably enhanced fluxes during some periods at those sites.

FLEXPART Atmospheric Transport and Deposition Model Simulations. To investigate the origins of the lead deposited at the NGRIP2 ice-core site in Greenland and at the three European peat bog sites, we used the well-established Lagrangian particle dispersion model FLEXPART (20, 52–55), taking advantage of a unique new development (23) that allows running the model backward in time for dry and wet deposition quantities. As with the more typical backward calculations for atmospheric concentrations (56), the output of such model calculations is a source–receptor relationship that maps sensitivity of the modeled deposition at the selected measurement (receptor) site (i.e., NGRIP2, Myrarnar, Flanders Moss, or Penido Vello) to an emission (source) flux. With a prescribed emission field (or, as in this case, potentially a point emission source), lead deposition can be calculated by multiplying the model output with the emission flux.

The model was run in backward mode at monthly intervals for the period 1901 through 1999, and particles were traced backward for 30 d, corresponding to several times the average lifetime of the tracked aerosol. Lacking the detailed meteorological fields during antiquity necessary for modeling, we used the recently completed coupled climate reanalysis for the 20th century (CERA-20C) (57) performed at the European Centre for Medium Range Weather Forecasts. We used the reanalysis data at a resolution of 2° × 2° and every 6 h. For further analysis, we excluded the first 20 y of the simulations because of a discontinuity in CERA-20C precipitation at the NGRIP2 location and a resulting step change in deposition flux around 1920. The sparsity of air pressure observations in the first two decades may render the reanalysis before 1920 less reliable than for later years.

Lead attaches to ambient background aerosol, and we assumed that this aerosol consisted mainly of mineral dust (logarithmic mean diameter of 1 μm and SD of 0.9), which may preexist in the atmosphere or be comobilized with lead. The choice of the aerosol type was supported by the fact that observed dust tracers were correlated with lead in the ice core. To test sensitivity of the results to the assumed ambient aerosol type, we also performed separate calculations for mineral dust with logarithmic mean diameters of 5 μm (SD 0.9), as well as sulfate and black carbon aerosols with assumed logarithmic mean diameters of 0.4 μm (SD of 0.3). The 1920 through 1999 average emissions sensitivities for Rio Tinto (37°N, 7°W) (Fig. 1) in southern Spain for the 1-μm dust, sulfate, and black carbon aerosols were 12.9, 8.4, and 10.3 μg/m^2/a, respectively, all with 58% year-to-year variability. Sensitivity and variability were 200% greater for the larger 5-μm dust aerosol.

We also calculated the ratio of emissions sensitivity for the peat bog sites with that for NGRIP2 (Fig. S5). Results suggested that only sources in southwestern Europe or northwestern Africa were consistent with the factor 100–1,000 higher measured deposition rates at the European peat bog sites than at NGRIP2 (i.e., the ancient Chinese empires probably were not significant contributors to the Greenland ice or European bog lead records).

Estimated Lead Emissions Using Nonbackground Lead Deposition and Modeling. By assuming (*i*) a single emission location in the Rio Tinto area (37°N, 7°W) (Fig. 1) and (*ii*) that atmospheric circulation and lead deposition processes were similar to those from 1920 to 1999 when the detailed atmospheric fields necessary for FLEXPART modeling were available from reanalyses (CERA-20C), we estimated the lead emissions from the observed deposition of pollution lead in Greenland from 1100 BCE to 800 CE. The FLEXPART simulations indicated that a 1-kg/s lead emission source in southern Spain would yield average pollution lead deposition of 12.9 μg/m^2/a in central Greenland. The magnitude of this conversion factor depends heavily on the scavenging properties of the aerosol and the precipitation input used by FLEXPART, so it may be subject to systematic biases in the model. Based on differences between the four different model tracers evaluated in FLEXPART, we estimated an uncertainty in the overall magnitude of the lead emissions of a factor of two.

Year-to-year variability (1 σ) in FLEXPART-simulated atmospheric transport and deposition was 7.5 μg/m^2/a or 58% of the mean. To reduce the year-to-year variability attributed to variations in atmospheric transport and deposition while preserving any step-function changes, we evaluated the measured annual lead deposition rates and estimated emissions after filtering with an 11-y median filter. Applying the same 11-y median filter to the model-simulated annual deposition from a constant source resulted in an estimated variability (1 σ) in deposition and emissions in central Greenland of 22% (Fig. 3).

While we modeled transport and deposition of lead aerosols from a single idealized emissions source in southern Spain (37°N, 7°W) to central Greenland using FLEXPART, the model simulations showed that emissions sensitivities at NGRIP2 for known ancient mining sites south of 40°N were relatively constant (21% coefficient of variation) throughout the western and northern Mediterranean region (Fig. S6). Therefore, lead emissions or a combination of emissions from any of these mining sites would have yielded similar levels of pollution deposition at NGRIP2. Emissions sensitivities at mining sites between 40 and 50°N (e.g., northern Spain) were somewhat higher (∼150%) than those at southern Spain, while those north of 50°N (e.g., Britain) were substantially higher (∼400%) and would have yielded higher pollution deposition per unit emission. Published estimates of lead production from 50 BCE to 500 CE based on historical and archaeological sources (18), however, indicated that British levels were only 10% of those in Iberia, suggesting that the NGRIP2 lead pollution record still was dominated by Iberian emissions. Emissions sensitivities for the southern and eastern Mediterranean (Fig. S6), including the Greek-era mining region of Laurion, were substantially lower (∼14% of those in southern Spain), meaning that the NGRIP2 lead pollution record was relatively insensitive to lead emissions from Laurion and surrounding regions.

ACKNOWLEDGMENTS. We thank S. Bernard and M. Legrand for helpful comments; R. Kreidberg for editorial assistance; the North Greenland Ice Core Project (NGRIP) community for providing ice-core samples; and students in the

Desert Research Institute ice-core laboratory for their assistance. Analysis and interpretation of archived NGRIP2 ice-core samples were supported by the John Fell Oxford University Press Research Fund and All Souls College, Oxford, as well as the Desert Research Institute. NGRIP is a multinational research program funded by participating institutions in Denmark, Germany, Japan, Sweden, Switzerland, France, Belgium, Iceland, and the United States.

1. Hong S, Candelone J, Patterson C, Boutron C (1996) History of ancient copper smelting pollution during Roman and medieval times recorded in Greenland ice. *Science* 272: 246–249.
2. Rosman K, Chisholm W, Hong S, Candelone J, Boutron C (1997) Lead from Carthaginian and Roman Spanish mines isotopically identified in Greenland ice dated from 600 BC to 300 AD. *Environ Sci Technol* 31:3413–3416.
3. Hong S, Candelone JP, Patterson CC, Boutron CF (1994) Greenland ice evidence of hemispheric lead pollution two millennia ago by Greek and Roman civilizations. *Science* 265:1841–1843.
4. Wilson AI (2002) Machines, power and the ancient economy. *J Roman Stud* 92:1–32.
5. Kehoe D (2008) The early Roman empire: Production. *The Cambridge Economic History of the Greco-Roman World*, eds Scheidel W, Morris I, Saller RP (Cambridge Univ Press, Cambridge, UK), pp 543–569.
6. de Callataÿ F (2005) The Graeco-Roman economy in the super long-run: Lead, copper and shipwrecks. *J Roman Archaeol* 18:361–372.
7. McConnell JR, et al. (2014) Antarctic-wide array of high-resolution ice core records reveals pervasive lead pollution began in 1889 and persists today. *Sci Rep* 4:5848.
8. McConnell JR, Edwards R (2008) Coal burning leaves toxic heavy metal legacy in the Arctic. *Proc Natl Acad Sci USA* 105:12140–12144.
9. Martinez Cortiza A, et al. (2002) Atmospheric Pb deposition in Spain during the last 4600 years recorded by two ombrotrophic peat bogs and implications for the use of peat as archive. *Sci Total Environ* 292:33–44.
10. Cloy J, Farmer J, Graham M, MacKenzie A, Cook G (2008) Historical records of atmospheric Pb deposition in four Scottish ombrotrophic peat bogs: An isotopic comparison with other records from western Europe and Greenland. *Global Biogeochem Cycles* 22:GB2016.
11. Shotyk W, et al. (2005) Accumulation rates and predominant atmospheric sources of natural and anthropogenic Hg and Ph on the Faroe Islands. *Geochim Cosmochim Acta* 69:1–17.
12. Renberg I, Persson MW, Emteryd O (1994) Preindustrial atmospheric lead contamination detected in Swedish lake sediments. *Nature* 368:323–326.
13. Pompeani DP, Abbott MB, Steinman BA, Bain DJ (2013) Lake sediments record prehistoric lead pollution related to early copper production in North America. *Environ Sci Technol* 47:5545–5552.
14. Sigl M, et al. (2015) Timing and climate forcing of volcanic eruptions for the past 2,500 years. *Nature* 523:543–549.
15. Matsumoto A, Hinkley TK (2001) Trace metal suites in Antarctic pre-industrial ice are consistent with emissions from quiescent degassing of volcanoes worldwide. *Earth Planet Sci Lett* 186:33–43.
16. Adolphi F, Muscheler R (2016) Synchronizing the Greenland ice core and radiocarbon timescales over the Holocene–Bayesian wiggle-matching of cosmogenic radionuclide records. *Clim Past* 12:15–30.
17. Patterson CC (1972) Silver stocks and losses in ancient and medieval times. *Econ Hist Rev* 25:205–233.
18. Nriagu JO (1983) *Lead and Lead Poisoning in Antiquity* (Wiley, New York).
19. Craddock PT, Hughes M; British Museum, Department of Scientific Research; Historical Metallurgy Society; British Museum, Research Laboratory (1985) *Furnaces and Smelting Technology in Antiquity* (British Museum, Department of Scientific Research, London).
20. Stohl A, Forster C, Frank A, Seibert P, Wotawa G (2005) Technical note: The Lagrangian particle dispersion model FLEXPART version 6.2. *Atmos Chem Phys* 5: 2461–2474.
21. Wilson A, Friedman H (2010) Mining Database. Version 1.0. Available at oxrep.classics.ox.ac.uk/databases/mines_database/. Accessed May 21, 2017.
22. Wilson AI (2007) The metal supply of the Roman Empire. *Supplying Rome and the Roman Empire*, ed Papi E (JRA Supplement 69,) (Journal of Roman Archaeology, Portsmouth, RI), pp 102–125.
23. Eckhardt S, et al. (2017) Source-receptor matrix calculation for deposited mass with the Lagrangian particle dispersion model FLEXPART v10.2 in backward mode. *Geophys Model Dev* 10:4605–4618.
24. Giardino C (2014) *Mineral Resources and Mines of Etruria* (Routledge, London).
25. Chamorro JG (1987) Survey of archaeological research on Tartessos. *Am J Archaeol* 91: 197–232.
26. Harl KW (1996) *Coinage in the Roman Economy, 300 B.C. To A.D. 700* (Johns Hopkins Univ Press, Baltimore).
27. Richardson JS (1986) *Hispaniae: Spain and the Development of Roman Imperialism, 218-82 BC* (Cambridge Univ Press, Cambridge, UK).
28. Perrin B (1919) *Plutarch's Lives* (W. Heinemann, London).
29. Harper K (2017) *The Fate of Rome: Climate, Disease, and the End of an Empire* (Princeton Univ Press, Princeton, NJ).
30. Blanchard I (2001) *Mining, Metallurgy and Minting in the Middle Ages* (Franz Steiner, Stuttgart, Germany).
31. Butcher K, Ponting M (2015) *The Metallurgy of Roman Silver Coinage: From the Reform of Nero to the Reform of Trajan* (Cambridge Univ Press, Cambridge, UK).
32. More AF, et al. (2017) Next-generation ice core technology reveals trye minimum natural levels of lead (Pb) in the atmosphere: Insights from the Black Death. *GeoHealth* 1:211–219.
33. Rasmussen S, et al. (2006) A new Greenland ice core chronology for the last glacial termination. *J Geophys Res Atmos* 111:D06102.
34. McConnell JR, Lamorey GW, Lambert SW, Taylor KC (2002) Continuous ice-core chemical analyses using inductively coupled plasma mass spectrometry. *Environ Sci Technol* 36:7–11.
35. McConnell JR, et al. (2017) Synchronous volcanic eruptions and abrupt climate change ~17.7 ka plausibly linked by stratospheric ozone depletion. *Proc Natl Acad Sci USA* 114:10035–10040.
36. McConnell JR, Aristarain AJ, Banta JR, Edwards PR, Simões JC (2007) 20th-century doubling in dust archived in an Antarctic Peninsula ice core parallels climate change and desertification in South America. *Proc Natl Acad Sci USA* 104:5743–5748.
37. Rhodes RH, et al. (2015) Paleoclimate. Enhanced tropical methane production in response to iceberg discharge in the North Atlantic. *Science* 348:1016–1019.
38. McConnell JR, et al. (2007) 20th-century industrial black carbon emissions altered Arctic climate forcing. *Science* 317:1381–1384.
39. Arienzo MM, et al. (2016) A method for continuous (239)Pu determinations in Arctic and Antarctic ice cores. *Environ Sci Technol* 50:7066–7073.
40. Hinkley TK, Lamothe PJ, Wilson SA, Finnegan DL, Gerlach TM (1999) Metal emissions from Kilauea, and a suggested revision of the estimated worldwide metal output by quiescent degassing of volcanoes. *Earth Planet Sci Lett* 170:315–325.
41. Bowen H (1966) *Trace Elements in Biochemistry* (Academic, New York).
42. Rhodes R, Baker J, Millet M, Bertler N (2011) Experimental investigation of the effects of mineral dust on the reproducibility and accuracy of ice core trace element analyses. *Chem Geol* 286:207–221.
43. Uglietti C, Gabrielli P, Olesik J, Lutton A, Thompson L (2014) Large variability of trace element mass fractions determined by ICP-SFMS in ice core samples from worldwide high altitude glaciers. *Appl Geochem* 47:109–121.
44. Patterson CC, Settle DM (1987) Magnitude of lead flux to the atmosphere from volcanoes. *Geochim Cosmochim Acta* 51:675–681.
45. Nriagu JO (1979) Global inventory of natural and anthropogenic emissions of trace metals to the atmosphere. *Nature* 279:409–411.
46. Andersen K, et al. (2006) The Greenland ice core chronology 2005, 15-42 ka. Part 1: Constructing the time scale. *Quat Sci Rev* 25:3246–3257.
47. Plummer C, et al. (2012) An independently dated 2000-yr volcanic record from Law Dome, East Antarctica, including a new perspective on the dating of the 1450s CE eruption of Kuwae, Vanuatu. *Clim Past* 8:1929–1940.
48. Wolff E, Moore J, Clausen H, Hammer C (1997) Climatic implications of background acidity and other chemistry derived from electrical studies of the Greenland Ice Core Project ice core. *J Geophys Res Oceans* 102:26325–26332.
49. Sigl M, et al. (2014) Insights from Antarctica on volcanic forcing during the Common Era. *Nat Clim Change* 4:693–697.
50. Martinez Cortizas A, Pontevedra Pombal X, Novoa Munoz JC, Garcia Rodeja E (1997) Four thousand years of atmospheric Pb, Cd, and Zn deposition recorded by the ombrotrophic peat bog of Penido Vello (Northwestern Spain). *Water Air Soil Pollut* 100:387–403.
51. Bindler R, Klarqvist M, Klaminder J, Forster J (2004) Does within-bog spatial variability of mercury and lead constrain reconstructions of absolute deposition rates from single peat records? The example of Store Mosse, Sweden. *Global Biogeochem Cycles* 18:GB3020.
52. Grythe H, et al. (2017) A new aerosol wet removal scheme for the Lagrangian particle model FLEXPART v10. *Geosci Model Dev* 10:1447–1466.
53. Stohl A, Hittenberger M, Wotawa G (1998) Validation of the Lagrangian particle dispersion model FLEXPART against large-scale tracer experiment data. *Atmos Environ* 32:4245–4264.
54. Stohl A, et al. (2007) Arctic smoke—Record high air pollution levels in the European Arctic due to agricultural fires in Eastern Europe in spring 2006. *Atmos Chem Phys* 7: 511–534.
55. Stohl A, et al. (2013) Black carbon in the Arctic: The underestimated role of gas flaring and residential combustion emissions. *Atmos Chem Phys* 13:8833–8855.
56. Seibert P, Frank A (2004) Source-receptor matrix calculation with a Lagrangian particle dispersion model in backward mode. *Atmos Chem Phys* 4:51–63.
57. Laloyaux P, de Boisseson E, Dahlgren P (2017) CERA-20C: An Earth system approach to climate reanalysis. *ECMWF Newsletter* 150:25–30.